J. Innovative Eng. Nat. Sci., vol. 6, no. 2, pp. 611-625, 2026.
http://doi.org/10.61112/jiens.1850543

Journal of Innovative Engineering and Natural Science
(Yenilikçi Mühendislik ve Doğa Bilimleri Dergisi)
https://dergipark.org.tr/en/pub/jiens

Original Paper

Comparative fractographic assessment of stiffness gain and strength retention in waste-cellulose-reinforced PLA composites

Kaan Bilge [a*]

[a]*Department of Aeronautical Engineering, Istanbul Technical University, Maslak, Istanbul and, Türkiye.*

ARTICLE INFO

Article history:
Received April 2, 2026
Received in revised form June 22, 2026
Accepted July 18, 2026

Available online

Keywords:
Polylactic Acid
Green Composites
Cellulose
Mechanical Behavior
Fractography

ABSTRACT

Cellulosic PLA composites are often evaluated mainly through stiffness increase, although stiffness alone does not show whether reinforcement produces useful strengthening or an embrittled crack path. This work presents a comparative failure-analysis study of two published waste-cellulose-fiber (WCF)/PLA systems processed by thermokinetic high-shear mixing and injection molding but based on different PLA grades and processing states. The common formulations of neat PLA, 10 wt.% WCF, 20 wt.% WCF, and 30 wt.% WCF are re-examined using tensile data, supplier datasheet context, and comparative SEM fractography. Both routes showed strong WCF-induced stiffening, but their strength responses diverged. In the 4043D-type route, 10, 20, and 30 wt.% WCF increased tensile modulus by approximately 45%, 68%, and 102%, respectively, while tensile strength increased by approximately 30%, 46%, and 56%. In the same sequence, strain at break changed by approximately +1%, −28%, and −37%. In the L130-type route, 10, 20, and 30 wt.% WCF increased tensile modules by approximately 43%, 83%, and 116%, respectively, but tensile strength remained below the neat-matrix value, decreasing by approximately 28%, 12%, and 7%. Strain at break also decreased by approximately 40%, 36%, and 36%. Fractography shows that this divergence corresponds to different failure styles: the 4043D-type route retains rougher fracture topography, matrix shearing, fibrillation, and deformation-accommodating debonding, whereas the L130-type route shows smoother lamellar regions, fiber-adjacent cracking, local fiber fracture, and broader block-like separation. The study therefore demonstrates that similar modulus gains across 10–30 wt.% WCF can arise from different fracture architectures. For WCF/PLA composites, processing history, matrix state, and fracture morphology should be reported together with tensile property changes to distinguish strengthening from stiffness-driven embrittlement.

I. INTRODUCTION

Polylactic acid (PLA) remains one of the most widely used bio-based thermoplastics because it combines renewable origin, relatively high stiffness, and compatibility with conventional melt-processing routes such as extrusion and injection molding [1–5]. These characteristics have moved PLA beyond packaging and disposable products toward lightweight structural and semi-structural composite applications, especially where reduced fossil-resource dependence and thermoplastic processability are both required [6, 7]. However, PLA should not be treated as a single interchangeable matrix. Its crystallization behavior, thermal history, molecular architecture, and processing-induced morphology strongly influence stiffness, strength, ductility, and failure mode [8–12]. For composite design, this means that fiber loading alone cannot explain mechanical performance unless the matrix grade and processing state are also considered.

Natural-fiber and cellulose-reinforced PLA composites are often presented as scalable routes for improving stiffness while maintaining a bio-based material profile [13–16]. In these systems, modulus improvement is comparatively easy to obtain because cellulose-derived fibers and fillers introduce a rigid dispersed phase into the polymer. Strength improvement is less automatic. It depends on fiber dispersion, fiber length retention, interfacial adhesion, void content, matrix continuity, and the ability of the fiber-adjacent PLA to deform without early crack

*Corresponding author. Tel.: +90-533-426-7487; e-mail: kaanbilge@itu.edu.tr

localization. Studies on PLA and related thermoplastic composites show that changes in reinforcement morphology, interface quality, and processing route can produce very different mechanical outcomes even when the nominal filler content is similar [17–21]. Therefore, the central issue is not whether cellulose can stiffen PLA, but whether the resulting fiber–matrix architecture can also sustain tensile load without premature damage localization.

Processing history is particularly important because it defines the matrix state that surrounds the reinforcement. PLA melt rheology controls fiber wetting, melt continuity, and mold filling, while drying, thermal exposure, and molding conditions influence degradation and crystallization during processing [22–24]. This issue becomes more sensitive in cellulose-filled PLA because cellulosic reinforcements can retain moisture and introduce hydroxyl-rich surfaces into the melt. Residual moisture can promote hydrolytic chain scission, reduce molecular weight, alter viscosity, and weaken the matrix before mechanical loading begins [25, 26]. Processing parameters such as shear, residence time, cooling path, and thermal profile can therefore convert a nominally reinforcing cellulose phase into either a load-sharing network or a crack-promoting defect population [27, 28].

The range of reported mechanical responses in PLA/cellulose composites reflects this coupling between reinforcement and matrix state. Cellulose nanofibers, cellulose nanofibril networks, hemp fibers, chemically treated wood fibers, and wood-derived fillers can all increase stiffness, but their effects on tensile strength and strain at break are more conditional [29–33]. When dispersion and interfacial stress transfer are sufficient, cellulose can delay damage accumulation and support strengthening. When agglomeration, debonding, poor wetting, moisture-related defects, or excessive matrix constraint dominate, stiffness increases may occur together with strength loss and embrittlement. This stiffness–strength separation is the main failure-analysis problem in cellulosic PLA composites.

Fractography is therefore essential for interpreting these systems. Tensile modulus and strength values describe the outcome, but fractured surfaces record the sequence by which load transfer breaks down. Features such as matrix fibrillation, ligament bridging, plastic tearing, fiber pull-out, fiber fracture, void growth, faceted fracture, lamellar splitting, and cleavage-like domains indicate whether the matrix redistributed stress before final separation or whether cracks localized early around fibers and interphase regions [34–41]. A rough and tortuous fracture surface with matrix drawing suggests a deformation-capable matrix and energy-dissipative failure. A flatter or more faceted surface with fiber-adjacent cracking suggests that reinforcement has promoted a more brittle crack path.

Several representative PLA/cellulose studies further show why matrix state must be considered together with fiber type. Natural fibers and wood-based reinforcements can improve stiffness and sometimes strength, but their effectiveness depends on fiber morphology, matrix compatibility, and the balance between fiber pull-out and matrix yielding [42–44]. Microcrystalline cellulose can act as an efficient stiffener, yet its strength contribution depends on dispersion quality and whether the PLA phase remains continuous between filler-rich regions [45]. These observations are especially relevant for waste-cellulose-fiber systems, where sustainability benefits are accompanied by variability in fiber size, surface condition, residual moisture, and thermal history. Published WCF/PLA datasets demonstrate that the same upcycled cellulose stream can produce strong stiffness gains, but the corresponding strength response depends strongly on the PLA matrix grade and crystallization history [46, 47].

Nanocellulosic PLA systems add the same message at a smaller length scale. Cellulose nanofibers, bacterial cellulose nanofibers, and cellulose nanofibril-based reinforcements can generate large interfacial area and significant stiffness enhancement at low loading [48–53]. However, this high interfacial area can either stabilize stress transfer or amplify embrittlement depending on dispersion, drying route, interphase formation, and crystallization behavior. Recent work on cellulose-fiber PLA, hemp/PLA, additively manufactured natural-fiber PLA, durable PLA biocomposites, and bark- or biomass-filled PLA confirms that reinforcement performance cannot be judged from filler content alone [54–61]. The mechanical response must be read through the combined effects of reinforcement geometry, matrix crystallinity, processing damage, and fracture morphology.

Crystallization is a key mechanism linking processing to failure. PLA crystallinity can improve stiffness and heat resistance, but it can also reduce plastic deformation and promote brittle fracture when crystalline domains constrain the matrix [62]. Cellulose-based fibers are known to influence polymer composite behavior through their surface chemistry, moisture sensitivity, interfacial bonding, and damage mechanisms [63, 64]. In PLA, fiber surfaces may also promote local crystalline organization, including transcrystalline or lamellar regions near the interface [65, 66]. Such fiber-adjacent crystalline regions can be beneficial if they improve stress transfer without suppressing matrix yielding but damaging if they form brittle shells that guide crack growth along the fiber–matrix interface. Interfacial modification and fiber–matrix compatibility are therefore not only adhesion issues; they also determine how crystallization, stress transfer, and fracture path interact [67, 68].

This work re-examines two published PLA/waste-cellulose-fiber composite systems through tensile-property comparison, supplier datasheet context, and SEM fractography. Rather than treating WCF content as the sole design variable, it frames WCF/PLA performance as a coupled stiffness–strength–fracture problem: fiber loading defines how much reinforcement is introduced, but matrix state, processing sensitivity, crystallization tendency, interphase morphology, and fiber-adjacent damage determine how the composite fails. The broader contribution is an adapted fractographic framework based on transferable failure signatures, including matrix shearing, fibrillation, deformation-accommodating debonding, fiber-adjacent cracking, lamellar separation, local fiber fracture, and block-like separation. These mechanisms may appear across many PLA grades and processing histories; what changes between PLA-based cellulosic composite systems is their relative dominance and sequence during crack growth.

II. EXPERIMENTAL METHOD / TEORETICAL METHOD

This work is a secondary analysis of published mechanical datasets combined with SEM fractography. No new compounding, pelletisation, DSC testing, or tensile testing was carried out. The comparison was restricted to the common formulation set of neat PLA, 10 wt.% WCF, 20 wt.% WCF, and 30 wt.% WCF. The first source study used Ingeo 4043D and was reported by Oguz et al. [46]. Waste cellulosic cotton fibers derived from the textile industry were supplied by Zorlu Linen Textile, Istanbul, Turkey. The average diameter of these fibers was measured as 15–20 μm [46-47]. Representative SEM images of employed WCF fibers are provided in figure 1a (general view) and figure 1b (single fiber view). Individual fiber length was not reliably determined because of strong entanglement in the as-received WCF.

The compounds were prepared by Gelimat thermokinetic mixing at 5200 rpm up to a melt temperature near 190 ºC, followed by injection molding at 190 ºC with a cold mold close to 30 ºC [46]. The second source study used

Luminy L130 and was reported by Ariturk et al. [47]. Only the WCF-only, zero-vermiculite subset was retained from that study, and the processing route again consisted of thermokinetic high-shear mixing followed by injection molding [47]. The two studies are therefore comparable in reinforcement type and overall processing family, but they are not a controlled head-to-head experiment because the matrix grade and processing state differ.

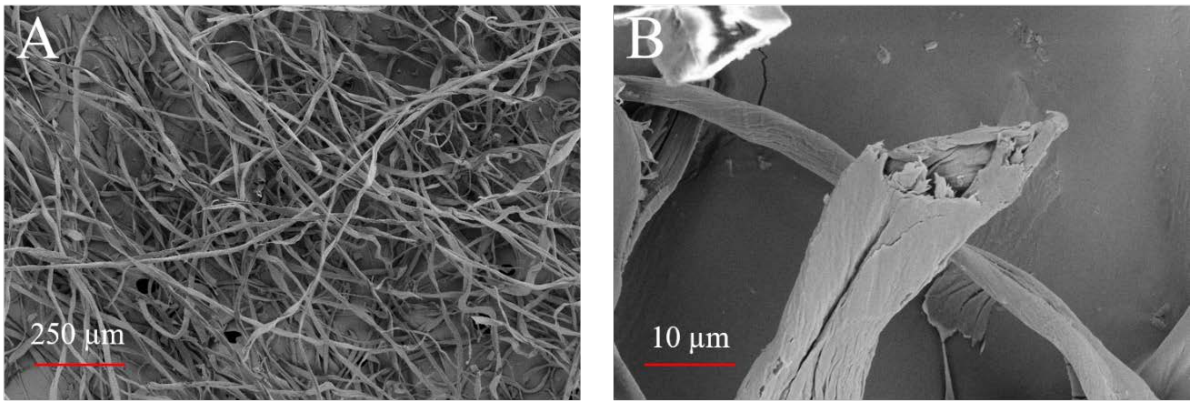

Figure 1: Views from employed WCF at reference studies [46] and [47]. A) Overall view from as purchased upcycled WCF b) Single WCF fiber

Table 1 provides the supplier datasheet context together with the key characterization procedures reported in the two source studies. The most important contrast for the present discussion is melt flow rate: Ingeo 4043D is reported at 6 g/10 min, whereas Luminy L130 is reported at 23 g/10 min under the same test condition [23, 24]. Read together with the cold-molding history and the fracture evidence, this difference supports the comparative interpretation used throughout the paper: the L130 route began from a more flowable matrix state and was more prone to localized cracking after fiber addition, whereas the lower-MFR 4043D route remained more deformation-accommodating [22, 9, 11].

Table 1. Supplier datasheet properties and key characterization procedures used to contextualize the two PLA grades and the two source studies

Property / Procedure	Ingeo 4043D (NatureWorks)	Luminy L130 (Total Corbion)
Density (g/cm³)	1.24	1.24
Melt flow rate	6 g/10 min (210 °C/2.16 kg)	23 g/10 min (210 °C/2.16 kg)
T_g (DSC, °C)	55–60	60
T_m (DSC, °C)	145–160	175
Tensile modulus (MPa)	3600	3500
Tensile strength (MPa)	60 (yield); 53 (break)	50
Elongation at break (%)	6	≤5
HDT (0.45 MPa, °C)	55	60 (amorph.); 105 (cryst.)
Drying recommendation	<250 ppm; 4 h @ 80 °C	<250 ppm (pref. <100); 4–6 h @ 100 °C
DSC instrument	TA Q2000 (indium-calibrated; Tzero)	DSC 3 + 700 (Mettler Toledo)
DSC atmosphere	N_2	N_2
DSC temperature program	20–250 °C; heating/cooling rates 10°C/min	25–230 °C; rate 10 °C/min
Mechanical tests (tensile)	Tensile: ISO 527; crosshead rate 2 mm/min; Zwick Z100 universal tester	Tensile: ISO 527–2; crosshead rate 2 mm/min; Instron 5982 UTM
Processing context	Thermokinetic mixing; injection moulded with a cold mould near 30 °C	Thermokinetic mixing; WCF-only subset retained from the published study; discussed here as a high-MFR PLA under cold-moulding history

Fracture surfaces were examined by SEM using a Leo Supra 35VP field-emission scanning electron microscope (Carl Zeiss AG, Jena, Germany) at Sabanci University.Low-magnification images were used to examine overall fracture topography and localization, whereas higher-magnification images were used to examine fiber debonding,

fiber pull-out, matrix deformation, fiber-adjacent cracking, and interface condition. The same feature language was used for both systems so that the fracture surfaces could be compared directly [34, 36, 38].

3.1 Mechanical Response

Table 2 and Figure 2 summarize the common-composition comparison. In both systems, tensile modulus increased strongly with WCF content: the 4043D-type route increased from 3079 to 6212 MPa, and the L130-type route increased from 3236 to 7002 MPa between neat PLA and 30 wt.% WCF. At the stiffness level alone, the two routes therefore look broadly similar and remain consistent with the usual cellulose-driven stiffening reported for PLA composites [15, 19, 25]. The decisive divergence appears in tensile strength.

Table 2. Mechanical properties of the two PLA/WCF systems at the common WCF contents used in the comparative analysis

Matrix route	WCF (wt.%)	Tensile modulus (MPa)	Tensile strength (MPa)	Strain at break (%)
4043D-type	0	3079 ± 154	60.8 ± 3.0	3.03 ± 0.03
4043D-type	10	4455 ± 223	78.8 ± 3.9	3.07 ± 0.04
4043D-type	20	5165 ± 258	88.9 ± 4.4	2.17 ± 0.04
4043D-type	30	6212 ± 310	94.6 ± 4.7	1.92 ± 0.04
L130-type	0	3236 ± 30	66.9 ± 0.1	2.50 ± 0.10
L130-type	10	4635 ± 176	48.5 ± 4.1	1.50 ± 0.30
L130-type	20	5908 ± 199	58.9 ± 3.4	1.60 ± 0.10
L130-type	30	7002 ± 342	62.4 ± 3.8	1.60 ± 0.10

In the 4043D-type route, strength increased continuously from 60.8 to 94.6 MPa as WCF content increased from 0 to 30 wt.%. In the L130-type route, strength dropped to 48.5 MPa at 10 wt.% WCF and recovered only partially to 62.4 MPa at 30 wt.%, remaining below the neat-matrix value. Thus, both systems achieved similar stiffness gains, but only one converted those gains into useful strengthening. Strain at break decreased in both routes, as expected after the addition of rigid cellulosic reinforcement [30-32].

The difference is that the 4043D-type route lost ductility while still gaining strength, whereas the L130-type route lost ductility and strength together. This is the central mechanical result of the study. It shows why modulus increase alone is insufficient for judging structural usefulness and why the fracture path must be examined directly. Figure 2 presents the mechanical trends directly. The figure shows that both routes stiffened in a broadly similar way, but their strength trajectories diverged strongly after fiber addition. This divergence is consistent with the general observation that cellulose reinforcement in PLA tends to raise modulus more reliably than tensile strength, because the strength response is much more sensitive to interface condition and matrix continuity [14, 19, 33].

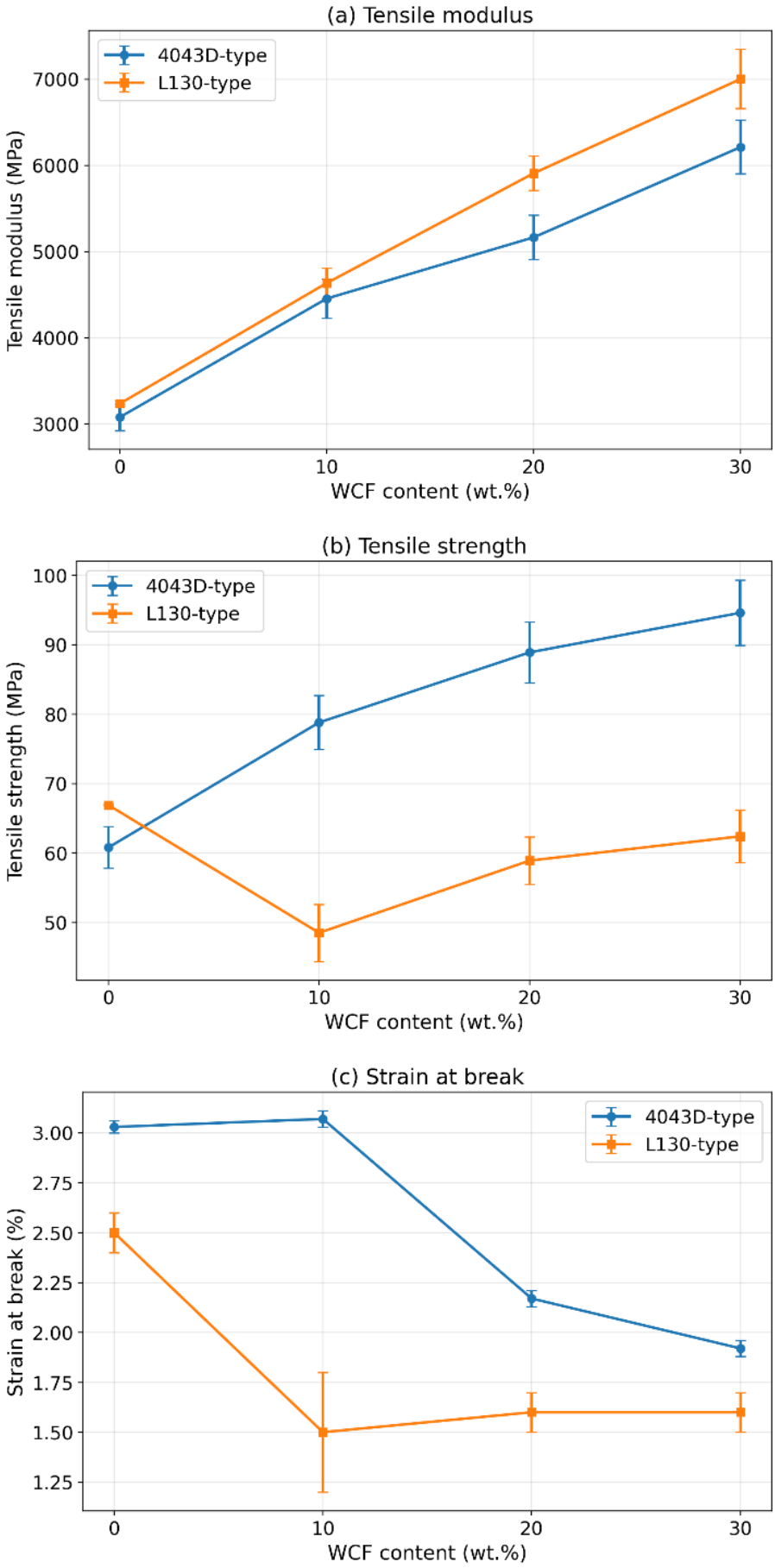

Figure 2. Comparative property trends in investigated works [46] and [47] a) Tensile modulus b) Tensile strength c) Strain at break

3.2 Comparative Macroscale Fractography

Figure 3 provides the first mechanistic explanation for the tensile divergence. In failure analysis, macroscale fractography is not merely descriptive; it is used to identify the dominant geometry of crack advance, the degree of crack-path interruption, and whether final separation occurred through a deformation-accommodating or a cracking-dominated route. Standard fractography texts for polymers and polymer composites treat roughness, ridge development, lamellar smoothness, fiber-related pull-out traces, and block-like separation as load-bearing clues rather than cosmetic features because they record how the crack front interacted with the surrounding microstructure during growth [34, 37, 40]. At the broadest scale, the 4043D-type route shows a rougher fracture topography with more pronounced ridges and relief in Figure 3A, whereas the L130-type route shows flatter and smoother regions with a more lamellar visual character in Figure 3B.

In macroscale fractography, increased roughness generally indicates that the crack front was repeatedly deflected, locally arrested, or forced to bridge across ligaments and heterogeneities before full separation. By contrast, smoother regions indicate a more planar crack path and a smaller degree of geometric interruption during propagation [34, 37, 40]. The neat matrices therefore already suggest different baseline crack-growth architectures before WCF is introduced: the 4043D-type route begins from a more topographically interrupted path, while the L130-type route begins from a path that is visually flatter and therefore more compatible with localized crack advance. Fiber debonding, pull-out traces, and matrix shearing Once WCF is added, the first key feature is the character of fiber-related damage.

At 10 wt.% WCF, the 4043D-type route shows fiber debonding together with matrix shearing in Figure 3C. This combination is important. Debonding alone does not imply poor structural behavior; in fractography it can also indicate that the interface separated only after the surrounding matrix had already deformed and redistributed stress. The associated sheared matrix regions therefore indicate that the interface was embedded in a still-participating matrix ligament system [31, 32, 34, 40].

In the L130-type route, debonding is coupled more directly to matrix cracking in Figure 3D. That change in association matters because it means the interface behaves less like a dissipative sliding/deformation zone and more like a preferred crack-initiation site. This distinction is consistent with the more mechanistic short-fiber PLA literature. Mazzanti et al. linked tensile response in PLA/hemp systems to fiber morphology and interfacial condition, showing that reinforcement efficiency depends on whether the fiber population promotes stress transfer or instead leaves a deboned-and-pull-out-dominated structure [31].

Csizmadia et al. similarly showed that strength improvement in PLA/wood systems required a change in fiber surface state, which is fully compatible with a fractographic reading based on better interfacial stress transfer and delayed separation [32]. Those studies support the present interpretation that fiber traces must be read together with the surrounding matrix morphology, not in isolation. Void coalescence, fibrillation, and ligament-controlled separation At 20 wt.% WCF, the 4043D-type route still contains void coalescence and matrix fibrillation in Figure 3E.

In polymer fractography, fibrillation and stretched ligaments are classic signs that the matrix carried load beyond initial damage and that crack advance required local drawing or tearing of polymer bridges.

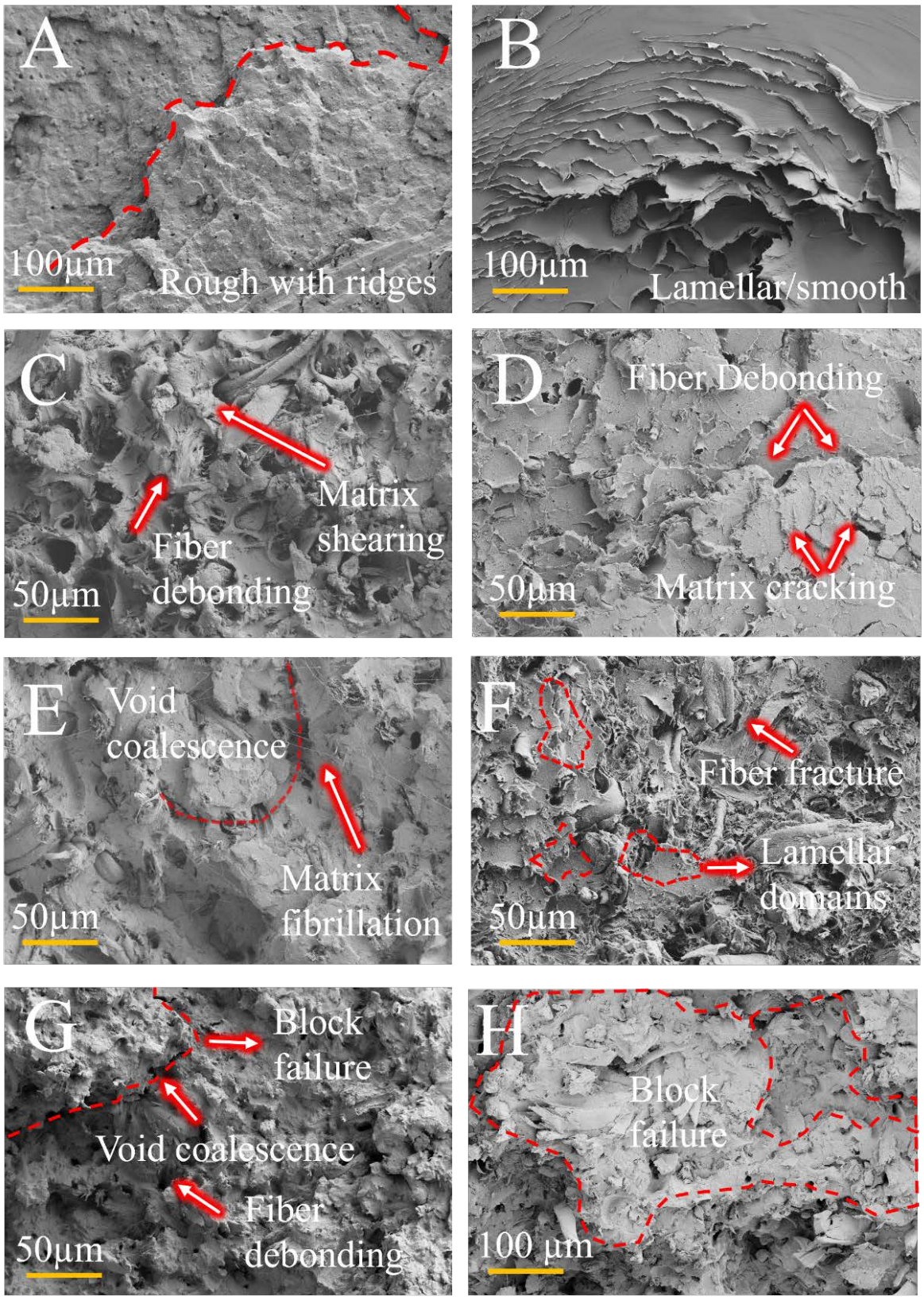

Figure 3. Comparative macroscale SEM fractography of PLA/WCF composites. The left column (A, C, E, G) shows the 4043D-type matrix and the right column (B, D, F, H) shows the L130-type matrix, at 0 (neat), 10, 20, and 30 wt.% WCF from top to bottom. (A) Neat 4043D: rough topography with pronounced ridges. (B) Neat L130: flatter, lamellar/smooth surface. (C) 4043D, 10 wt.%: fiber debonding with matrix shearing. (D) L130, 10 wt.%: fiber debonding coupled to matrix cracking. (E) 4043D, 20 wt.%: void coalescence with matrix fibrillation. (F) L130, 20 wt.%: local fiber fracture with smoother lamellar domains. (G) 4043D, 30 wt.%: block-like separation coexisting with voids and debonded regions. (H) L130, 30 wt.%: broader block-like separation with smooth lamellar areas. Scale bars as indicated on each panel.

Void coalescence in this context does not simply mean brittle cavitation; when accompanied by fibrillation it more often indicates progressive ligament thinning and local energy dissipation before final rupture [34, 39]. These are therefore deformation-bearing features. They imply that although damage was already present, the fracture path still advanced through repeated micro-interruption rather than through immediate planar separation. The L130-type route at the same loading level instead shows local fiber fracture together with smoother lamellar domains in Figure 3F.

In composite fractography, local fiber fracture is often a sign that load partitioning became more concentrated and that the crack front encountered fewer deformable matrix ligaments able to relax the local stress field. When this occurs together with flatter or lamellar polymer regions, the fracture path is better described as discontinuous and crack-dominant than as ductile tearing [36, 37, 40]. The macroscale implication is that the two systems reach similar stiffness increases through different damage sequences: one still supported by local matrix drawing, the other increasingly governed by crack linking between constrained regions. Lamellar regions and block-like separation At the highest loading level, both systems localize more strongly, but they do not localize in the same manner.

The 4043D-type route still fractures through a rougher, mechanically interrupted path in which block formation coexists with voids and deboned regions in Figure 3G. The L130-type route exhibits broader block-like separation and smoother lamellar areas in Figure 3H. In fractographic terms, block-like separation indicates that the fracture process became less dependent on distributed ligament tearing and more dependent on the joining of adjacent crack segments into larger contiguous zones. When paired with smoother lamellar regions, that morphology is usually interpreted as evidence that the matrix has lost much of its ability to stabilize crack growth through local deformation [34, 37, 39, 40].

For semi-crystalline polymers, lamellar smoothness is especially important because it often accompanies a reduction in plastic accommodation and a stronger tendency toward crack localization [39]. Read as a whole, Figure 3A–H therefore defines two different macroscale failure routes. The 4043D-type route is characterized by roughness, ridge development, debonding coupled to matrix shearing, and fibrillated ligament-controlled separation. The L130-type route is characterized by smoother lamellar areas, debonding coupled more directly to cracking, local fiber fracture, and broader block-like separation.

The first set of features is consistent with a deformation-accommodating crack path; the second is consistent with earlier crack localization and less effective interruption of crack advance. This is also where the present framework adds value relative to much of the broader cellulosic-PLA literature. Several nanocellulose studies discuss morphology primarily in terms of dispersion and nucleation, which is useful for interpreting crystallization but does not by itself reconstruct the fracture path [29, 30]. By contrast, failure-analysis-oriented fractography allows the mechanical divergence to be restated as a path problem: both systems stiffen, but only one retains a macroscale fracture route in which deformation features remain prominent.

3.3 Comparative Microscale Fractography

Figure 4 resolves the same contrast at the fiber scale. At this magnification, the main question is no longer only where the crack passed, but how the fiber-adjacent polymer participated in the last stage of load transfer. For cellulosic reinforcements in thermoplastics, the interface is usually governed by a combination of wetting quality,

mechanical interlocking with the fiber surface, local constraint of polymer chains, and any crystalline reorganization that develops next to the fiber during cooling [63, 65, 66]. The present images are therefore interpreted conservatively: they do not measure interfacial shear strength directly, but they do show whether separation remained coupled to local matrix deformation or became associated with localized cracking.

In the 4043D-type route, the WCF is bordered by a visibly deformed polymer region in Figure 4A. Debonding occurred, but it occurred together with matrix deformation, which suggests that interfacial failure was not completely abrupt. In practical terms, the fiber surface appears to have remained engaged long enough for the surrounding PLA to shear and redistribute stress before final separation. For short cellulosic reinforcements in thermoplastics, this is usually the more favorable case: some debonding is still present, but it is accompanied by pull-out resistance, frictional sliding, and deformation of the neighboring matrix rather than by immediate crack release [31, 32, 64].

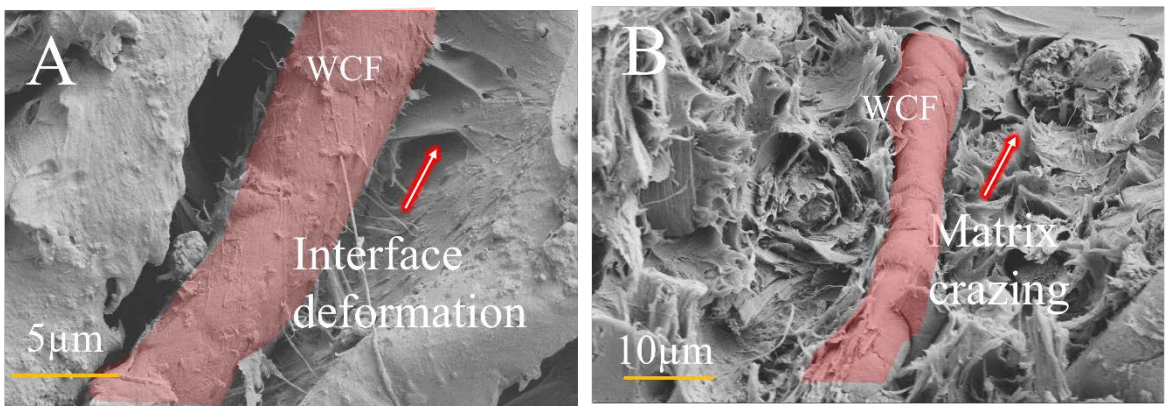

Figure 4: Comparative microscale fractography of fiber interfaces in the two PLA/WCF systems with 20 wt.% WCF. Panel A corresponds to the 4043D-type route and shows a waste-cellulose fiber (WCF) bordered by a locally deformed interface region, indicating that interfacial separation occurred together with visible matrix deformation. Panel B corresponds to the L130-type route and shows a waste-cellulose fiber surrounded by a more crack-dominated polymer region, where fine fibrillar microcracking is visible in the matrix adjacent to the fiber

By contrast, in the L130-type route the fiber-adjacent region is more crack-dominated, with fine fibrillar microcracking in the nearby polymer in Figure 4B. That morphology is more consistent with an interface region that no longer dissipates much deformation before the crack links through it. A second issue specific to cellulosic reinforcements in semicrystalline thermoplastics is that the fiber can act not only as a stress concentrator, but also as a crystallization site. Nanocellulose studies already cited in this manuscript show that cellulose can modify PLA through dispersion state, fibril-network formation, and nucleation-assisted crystallization [29, 30, 51].

At the microfiber scale, a related possibility is the development of a fiber-adjacent transcrystalline or transcrystalline-like region. Classical trans crystallinity literature makes clear that such interfacial layers are real morphological possibilities in semicrystalline polymer composites, but also that their effect on mechanical performance is system-dependent and should not be assumed a priori [66]. For PLA specifically, Wang et al. showed that sisal fibers can induce transcrystallization at the PLA interface under suitable crystallization conditions [65]. That literature supports a cautious interpretation here: the more ordered, crack-dominated fiber-adjacent regions in the L130-type route seen in Figure 4B are consistent with stronger interfacial crystallization effects, but the present SEM evidence alone does not prove a fully developed transcrystalline layer.

The broader PLA/natural-fiber interface literature is also useful in separating two different ideas that are often conflated. One is deliberate interface modification, where treatments are used to improve wetting and load transfer. The other is the actual damage path that remains after loading. Le Moigne et al., for example, linked optimized silane treatment in flax/PLA biocomposites to stronger interfacial bonding, reduced damping, and a shift toward more cohesive interfacial failure at higher loads, supported by in situ SEM crack-propagation observations [67].

That kind of study is valuable because it connects chemistry, interphase formation, and fractured evidence in one chain. The present WCF comparison addresses a different but related question: with no claim of interfacial strength measurement, the SEM signatures show whether the fiber-adjacent zone still deforms with the matrix or instead becomes a preferred crack-initiation region. In that sense, the 4043D-type route in Figure 4A looks closer to a tolerable debonding-and-drawing scenario, whereas the L130-type route in Figure 4B looks closer to a crack-localizing scenario. Taken together, the interface-scale observations in Figure 4A, B help explain the mechanical divergence without overextending the evidence.

In the 4043D-type route, interfacial separation is coupled to matrix deformation; in the L130-type route, it is coupled more strongly to localized cracking. Read together with Table 1, this supports the comparative interpretation that the higher-MFR L130 route, combined with cold molding, was less favorable for strength retention than the lower-MFR 4043D route [22, 9, 11]. The point is not that every fiber-adjacent crack in the L130-type route must arise from transcrystallinity, nor that every rougher interface in the 4043D-type route implies strong adhesion. Rather, the value of the fractographic framework is that it identifies the governing failure style at the interface: deformation-accommodating debonding versus crack-localizing separation.

IV. CONCLUSIONS

This study was presented as a comparative failure-analysis framework rather than as a property-only comparison. The two WCF/PLA source systems were then re-read through raw tensile data, datasheet context, and comparative SEM fractography so that their property divergence could be interpreted in terms of crack path rather than stiffness alone. Within that framework, both systems stiffened strongly with increasing WCF content, but they did not strengthen in the same way.

The 4043D-type route increased in modulus from 3.08 to 6.21 GPa and in tensile strength from 60.8 to 94.6 MPa, whereas the L130-type route increased in modulus from 3.24 to 7.00 GPa but remained below the neat-matrix strength after fiber addition. The fractographic evidence explains why. The 4043D-type route retained rougher fracture topography, matrix shearing, fibrillation, and deformation-accommodating debonding, which together indicate a more interruption-prone and strain-accommodating fracture path. The L130-type route showed smoother lamellar regions, fiber-adjacent cracking, local fiber fracture, and broader block-like separation, which are more consistent with earlier crack localization and linkage through fiber-bounded matrix regions.

The present work should be read as an adapted fractographic framework rather than as strictly controlled proof of a single matrix-driven mechanism. The two WCF/PLA systems compared here show how similar stiffness gains can be associated with different fracture routes, but the broader contribution is the definition of failure signatures that can be transferred to other PLA-based composite systems. Matrix shearing, fibrillation, deformation-accommodating debonding, fiber-adjacent cracking, lamellar separation, local fiber fracture, and block-like separation represent general fracture mechanisms that may appear across many PLA grades and processing

histories. What changes from one material system to another is not the existence of these mechanisms, but their relative dominance and sequence during crack growth. Future work should therefore combine this fractographic classification with controlled PLA grades, identical drying and molding histories, DSC-based crystallinity measurements, rheological characterization, and quantitative fiber–matrix interaction tests. Such studies would allow the failure mechanisms defined here to be linked more directly to crystallinity, matrix degradation, interfacial stress transfer, and strength retention.

ACKNOWLEDGMENT

The authors gratefully acknowledge the original experimental studies from which the mechanical data were taken [46, 47]. The authors also acknowledge Sabanci University Integrated Manufacturing Technologies Research and Application Center (SU IMC) for infrastructure support.

REFERENCES

1. Dorgan JR, Lehermeier HJ, Palade LI, Cicero J (2001) Polylactides: Properties and prospects of an environmentally benign plastic from renewable resources. Macromol Symp 175:55-66. https://doi.org/10.1002/1521-3900(200110)175:1<55::AID-MASY55>3.0.CO;2-K
2. Farah S, Anderson DG, Langer R (2016) Physical and mechanical properties of PLA, and their functions in widespread applications–A comprehensive review. Adv Drug Deliv Rev 107:367-392. https://doi.org/10.1016/j.addr.2016.06.012
3. Naser AZ, Deiab I, Darras BM (2021) Poly(lactic acid) (PLA) and polyhydroxyalkanoates (PHAs), green alternatives to petroleum-based plastics: A review. RSC Adv 11:17151-17196. https://doi.org/10.1039/D1RA02390J
4. Lim LT, Auras R, Rubino M (2008) Processing technologies for poly(lactic acid). Prog Polym Sci 33:820-852. https://doi.org/10.1016/j.progpolymsci.2008.05.004
5. Ahmed J, Varshney SK, Bini TB (2011) Polylactides–Chemistry, properties and green packaging technology: A review. Int J Food Prop 14:37-58. https://doi.org/10.1080/10942910903125284
6. Ramezani Dana H, Ebrahimi F (2023) Synthesis, properties, and applications of polylactic acid-based polymers. Polym Eng Sci 63:22-43. https://doi.org/10.1002/pen.26193
7. Nofar M, Sacligil D, Carreau PJ, Kamal MR, Heuzey MC (2019) Poly(lactic acid) blends: Processing, properties and applications. Int J Biol Macromol 125:307-360. https://doi.org/10.1016/j.ijbiomac.2018.12.002
8. Saeidlou S, Huneault MA, Li H, Park CB (2012) Poly(lactic acid) crystallization. Prog Polym Sci 37:1657-1677. https://doi.org/10.1016/j.progpolymsci.2012.07.005
9. Vadori R, Mohanty AK, Misra M (2013) The effect of mold temperature on the performance of injection molded poly(lactic acid)-based bioplastic. Macromol Mater Eng 298:981-990. https://doi.org/10.1002/mame.201200274
10. Harris AM, Lee EC (2008) Improving mechanical performance of injection molded PLA by controlling crystallinity. J Appl Polym Sci 107:2246-2255. https://doi.org/10.1002/app.27261
11. Yang H, Du J (2024) Crystallinity, rheology, and mechanical properties of low-/high-molecular-weight PLA blended systems. Molecules 29:169. https://doi.org/10.3390/molecules29010169
12. Aliotta L, Cinelli P, Coltelli MB et al (2022) Improvement of the PLA crystallinity and heat distortion temperature: Optimizing the content of nucleating agents and the injection molding cycle time. Polymers 14:977. https://doi.org/10.3390/polym14050977
13. Pickering KL, Efendy MGA, Le TM (2016) A review of recent developments in natural fibre composites and their mechanical performance. Compos Part A Appl Sci Manuf 83:98-112. https://doi.org/10.1016/j.compositesa.2015.08.038
14. Faruk O, Bledzki AK, Fink HP, Sain M (2012) Biocomposites reinforced with natural fibers: 2000–2010. Prog Polym Sci 37:1552-1596. https://doi.org/10.1016/j.progpolymsci.2012.04.003
15. Graupner N, Herrmann AS, Müssig J (2009) Natural and man-made cellulose fibre-reinforced poly(lactic acid) (PLA) composites: An overview about mechanical characteristics and application areas. Compos Part A Appl Sci Manuf 40:810-821. https://doi.org/10.1016/j.compositesa.2009.04.003

16. Siakeng R, Jawaid M, Ariffin H et al (2019) Natural fiber reinforced polylactic acid composites: A review. Polym Compos 40:446-463. https://doi.org/10.1002/pc.24747
17. Ariturk G, Bilge K, Seven SA, Menceloglu YZ (2024) Morphological adaptation of expanded vermiculite in polylactic acid and polypropylene matrices for superior thermoplastic composites. Polym Compos 45:5043-5050. https://doi.org/10.1002/pc.28108
18. van den Oever MJA, Beck B, Müssig J (2010) Agrofibre-reinforced poly(lactic acid) composites: Effect of moisture on degradation and mechanical properties. Compos Part A Appl Sci Manuf 41:1628-1635. https://doi.org/10.1016/j.compositesa.2010.07.011
19. Bledzki AK, Jaszkiewicz A, Scherzer D (2009) Mechanical properties of PLA composites with man-made cellulose and abaca fibres. Compos Part A Appl Sci Manuf 40:404-412. https://doi.org/10.1016/j.compositesa.2009.01.002
20. Haafiz MKM, Hassan A, Zakaria Z et al (2013) Properties of polylactic acid composites reinforced with oil palm biomass microcrystalline cellulose. Carbohydr Polym 98:139-145. https://doi.org/10.1016/j.carbpol.2013.05.069
21. Silva CG, Campini PAL, Rocha DB, Rosa DS (2019) The influence of treated eucalyptus microfibers on the properties of PLA biocomposites. Compos Sci Technol 179:54-62. https://doi.org/10.1016/j.compscitech.2019.04.010
22. Lehermeier HJ, Dorgan JR (2001) Melt rheology of poly(lactic acid): Consequences of blending chain architectures. Polym Eng Sci 41:2172-2184. https://doi.org/10.1002/pen.10912
23. NatureWorks LLC (2015) Ingeo™ Biopolymer 4043D technical data sheet. https://www.natureworksllc.com. Accessed 26 July 2026
24. TotalEnergies Corbion (2022) Product data sheet: Luminy® L130. https://totalenergies-corbion.com. Accessed 26 July 2026
25. Gorgun E, Ali A, Islam MS (2024) Biocomposites of poly(lactic acid) and microcrystalline cellulose: Influence of the coupling agent on thermomechanical and absorption characteristics. ACS Omega 9:11523-11533. https://doi.org/10.1021/acsomega.3c08448
26. Battegazzore D, Alongi J, Frache A (2014) Poly(lactic acid)-based composites containing natural fillers: Thermal, mechanical and barrier properties. J Polym Environ 22:88-98. https://doi.org/10.1007/s10924-013-0616-9
27. Mallet B, Lamnawar K, Maazouz A (2014) Improvement of blown film extrusion of poly(lactic acid): Structure–processing–properties relationships. Polym Eng Sci 54:840-857. https://doi.org/10.1002/pen.23610
28. Su Z, Li Q, Liu Y, Hu GH, Wu C (2009) Multiple melting behavior of poly(lactic acid) filled with modified carbon black. J Polym Sci Part B Polym Phys 47:1971-1980. https://doi.org/10.1002/polb.21790
29. Frone AN, Berlioz S, Chailan JF, Panaitescu DM (2013) Morphology and thermal properties of PLA–cellulose nanofibers composites. Carbohydr Polym 91:377-384. https://doi.org/10.1016/j.carbpol.2012.08.054
30. Gazzotti S, Rampazzo R, Hakkarainen M et al (2019) Cellulose nanofibrils as reinforcing agents for PLA-based nanocomposites: An in situ approach. Compos Sci Technol 171:94-102. https://doi.org/10.1016/j.compscitech.2018.12.015
31. Mazzanti V, Pariante R, Bonanno A et al (2019) Reinforcing mechanisms of natural fibers in green composites: Role of fibers morphology in a PLA/hemp model system. Compos Sci Technol 180:51-59. https://doi.org/10.1016/j.compscitech.2019.05.015
32. Csizmadia R, Faludi G, Renner K et al (2013) PLA/wood biocomposites: Improving composite strength by chemical treatment of the fibers. Compos Part A Appl Sci Manuf 53:46-53. https://doi.org/10.1016/j.compositesa.2013.06.003
33. Kamau-Devers K, Kortum Z, Miller SA (2019) Hydrothermal aging of bio-based poly(lactic acid) wood polymer composites: Studies on sorption behavior, morphology, and heat conductance. Constr Build Mater 214:290-302. https://doi.org/10.1016/j.conbuildmat.2019.04.098
34. Roulin-Moloney AC (ed) (1989) Fractography and failure mechanisms of polymers and composites. Elsevier Applied Science, London
35. Friedrich K (ed) (1989) Application of fracture mechanics to composite materials. Composite Materials Series, vol 6. Elsevier, Amsterdam
36. Purslow D (1986) Matrix fractography of fibre-reinforced epoxy composites. Composites 17:289-303. https://doi.org/10.1016/0010-4361(86)90746-9
37. Greenhalgh ES, Hiley MJ (2008) Fractography of polymer composites: Current status and future issues. 13th European Conference on Composite Materials (ECCM13), Stockholm, Sweden, Jun. 2-5.
38. Opelt CV, Cândido GM, Rezende MC (2018) Fractographic study of damage mechanisms in fiber reinforced polymer composites submitted to uniaxial compression. Eng Fail Anal 92:520-527. https://doi.org/10.1016/j.engfailanal.2018.06.009

39. Deblieck RAC, van Beek DJM, Remerie K, Ward IM (2011) Failure mechanisms in polyolefines: The role of crazing, shear yielding and the entanglement network. Polymer 52:2979-2990. https://doi.org/10.1016/j.polymer.2011.03.055
40. Greenhalgh ES (2009) Failure analysis and fractography of polymer composites. Woodhead Publishing, Cambridge. https://doi.org/10.1533/9781845696818
41. Hayes MD, Edwards DB, Shah AR (2015) Fractography in failure analysis of polymers. William Andrew, Oxford. ISBN 9780323353908
42. Bledzki AK, Jaszkiewicz A (2010) Mechanical performance of biocomposites based on PLA and PHBV reinforced with natural fibres–A comparative study to PP. Compos Sci Technol 70:1687-1696. https://doi.org/10.1016/j.compscitech.2010.06.005
43. Peltola H, Pääkkönen E, Jetsu P, Heinemann S (2014) Wood based PLA and PP composites: Effect of fibre type and matrix polymer on fibre morphology, dispersion and composite properties. Compos Part A Appl Sci Manuf 61:13-22. https://doi.org/10.1016/j.compositesa.2014.02.002
44. Fortunati E, Armentano I, Iannoni A, Kenny JM (2010) Development and thermal behaviour of ternary PLA matrix composites. Polym Degrad Stab 95:2200-2206. https://doi.org/10.1016/j.polymdegradstab.2010.02.034
45. Mathew AP, Oksman K, Sain M (2005) Mechanical properties of biodegradable composites from poly(lactic acid) and microcrystalline cellulose. J Appl Polym Sci 97:2014-2025. https://doi.org/10.1002/app.21779
46. Oguz O, Bilge K, Simsek E et al (2017) High performance green composites of poly(lactic acid) and waste cellulose fibers prepared by high-shear thermo-kinetic mixing. Ind Eng Chem Res 56:8568-8579. https://doi.org/10.1021/acs.iecr.7b02037
47. Ariturk G, Girisken C, Bilge K, Kovanci CY, Menceloglu YZ, Seven SA (2024) Hybrid green composites of PLA incorporated with upcycled waste cellulose and vermiculite. Eur Polym J 203:112667. https://doi.org/10.1016/j.eurpolymj.2023.112667
48. Iwatake A, Nogi M, Yano H (2008) Cellulose nanofiber-reinforced polylactic acid. Compos Sci Technol 68:2103-2106. https://doi.org/10.1016/j.compscitech.2008.03.006
49. Jonoobi M, Harun J, Mathew AP, Oksman K (2010) Mechanical properties of cellulose nanofiber (CNF) reinforced polylactic acid (PLA) prepared by twin screw extrusion. Compos Sci Technol 70:1742-1747. https://doi.org/10.1016/j.compscitech.2010.07.005
50. Panaitescu DM, Frone AN, Chiulan I, Gabor RA, Spataru IC, Casarica A (2017) Biocomposites from polylactic acid and bacterial cellulose nanofibers obtained by mechanical treatment. BioResources 12:662-672. https://doi.org/10.15376/biores.12.1.662-672
51. Shazleen SS, Yasim-Anuar TAT, Ibrahim NA, Hassan MA, Ariffin H (2021) Functionality of cellulose nanofiber as bio-based nucleating agent and nano-reinforcement material to enhance crystallization and mechanical properties of polylactic acid nanocomposite. Polymers 13:389. https://doi.org/10.3390/polym13030389
52. Gitari B, Chang BP, Misra M, Navabi A, Mohanty AK (2019) A comparative study on the mechanical, thermal, and water barrier properties of PLA nanocomposite films prepared with bacterial nanocellulose and cellulose nanofibrils. BioResources 14:1867-1889. https://doi.org/10.15376/biores.14.1.1867-1889
53. Collins A, Tajvidi M (2024) Cellulose nanofibrils dewatered with poly(lactic acid) for improved bio-polymer nanocomposite processing. Nanomaterials 14:1419. https://doi.org/10.3390/nano14171419
54. Graupner N, Müssig J (2017) Cellulose fiber-reinforced PLA versus PP. Int J Polym Sci 2017:6059183. https://doi.org/10.1155/2017/6059183
55. Srivastava P, Arumugam AB, Agrawal AP, Ntumba ZN (2025) Development of hemp fiber reinforced PLA composites for sustainable 3D printing: Mechanical and microstructural properties. J Nat Fibers. https://doi.org/10.1080/15440478.2025.2558214
56. Safdari F, Bagheriasl D, Carreau PJ, Heuzey MC, Kamal MR (2018) Rheological, mechanical, and thermal properties of polylactide/cellulose nanofiber biocomposites. Polym Compos 39:1752-1762. https://doi.org/10.1002/pc.24127
57. Sawpan MA, Pickering KL, Fernyhough A (2007) Hemp fibre-reinforced poly(lactic acid) composites. Adv Mater Res 29–30:337-340. https://doi.org/10.4028/www.scientific.net/AMR.29-30.337
58. Jing H, He H, Liu H, Huang B, Zhang C (2021) Study on properties of polylactic acid/lemongrass fiber biocomposites prepared by fused deposition modeling. Polym Compos 42:973-986. https://doi.org/10.1002/pc.25879
59. Stoof D, Pickering KL, Zhang Y (2017) Fused deposition modelling of natural fibre/polylactic acid composites. J Compos Sci 1:8. https://doi.org/10.3390/jcs1010008
60. Tripathi N, Misra M, Mohanty AK (2021) Durable polylactic acid (PLA) based sustainable engineered blends and biocomposites: Recent developments, challenges and opportunities. ACS Eng Au 1:7-38. https://doi.org/10.1021/acsengineeringau.1c00011

61. Borysiuk P, Boruszewski P, Auriga R et al (2021) Influence of a bark-filler on the properties of PLA biocomposites. J Mater Sci 56:9196-9208. https://doi.org/10.1007/s10853-021-05901-6
62. Ma B, Wang X, He Y, Dong Z, Zhang X, Chen X, Liu T (2021) Effect of poly(lactic acid) crystallization on its mechanical and heat resistance performances. Polymer 212:123280. https://doi.org/10.1016/j.polymer.2020.123280
63. Bledzki AK, Gassan J (1999) Composites reinforced with cellulose based fibres. Prog Polym Sci 24:221-274. https://doi.org/10.1016/S0079-6700(98)00018-5
64. Sydenstricker THD, Mochnaz S, Amico SC (2003) Pull-out and other evaluations in sisal-reinforced polyester biocomposites. Polym Test 22:375-380. https://doi.org/10.1016/S0142-9418(02)00116-2
65. Wang Y, Tong B, Hou S, Li M, Shen C (2011) Transcrystallization behavior at the poly(lactic acid)/sisal fibre biocomposite interface. Compos Part A Appl Sci Manuf 42:66-74. https://doi.org/10.1016/j.compositesa.2010.10.006
66. Quan H, Li ZM, Yang MB, Huang R (2005) On transcrystallinity in semi-crystalline polymer composites. Compos Sci Technol 65:999-1021. https://doi.org/10.1016/j.compscitech.2004.11.015
67. Le Moigne N, Longerey M, Taulemesse JM, Bénézet JC, Bergeret A (2014) Study of the interface in natural fibres reinforced poly(lactic acid) biocomposites modified by optimized organosilane treatments. Ind Crops Prod 52:481-494. https://doi.org/10.1016/j.indcrop.2013.11.022
68. Huang S, Fu Q, Yan L, Kasal B (2021) Characterization of interfacial properties between fibre and polymer matrix in composite materials – A critical review. J Mater Res Technol 13:1441-1484. https://doi.org/10.1016/j.jmrt.2021.05.076